

Embedded Graph Convolutional Networks for Real-Time Event Data Processing on SoC FPGAs

Kamil Jeziorek, Piotr Wzorek, Krzysztof Blachut, Andrea Pinna and Tomasz Kryjak *Senior Member IEEE*

Abstract—The utilisation of event cameras represents an important and swiftly evolving trend aimed at addressing the constraints of traditional video systems. Particularly within the automotive domain, these cameras find significant relevance for their integration into embedded real-time systems due to lower latency and energy consumption. One effective approach to ensure the necessary throughput and latency for event processing is through the utilisation of graph convolutional networks (GCNs). In this study, we introduce a custom EFGCN (Event-based FPGA-accelerated Graph Convolutional Network) designed with a series of hardware-aware optimisations tailored for PointNetConv, a graph convolution designed for point cloud processing. The proposed techniques result in up to 100-fold reduction in model size compared to Asynchronous Event-based GNN (AEGNN), one of the most recent works in the field, with a relatively small decrease in accuracy (2.9% for the N-Caltech101 classification task, 2.2% for the N-Cars classification task), thus following the TinyML trend. We implemented EFGCN on a ZCU104 SoC FPGA platform without any external memory resources, achieving a throughput of 13.3 million events per second (MEPS) and real-time partially asynchronous processing with low latency. Our approach achieves state-of-the-art performance across multiple event-based classification benchmarks while remaining highly scalable, customisable and resource-efficient. We publish both software and hardware source code in an open repository: <https://github.com/vision-agh/gcnn-dvs-fpga>.

Index Terms—Graph Convolutional Neural Networks, Event Cameras, Object Classification, FPGAs, Event-based Vision, Tiny Machine Learning.

I. INTRODUCTION

Embedded vision systems have become an integral part of many modern technologies, especially in advanced mobile robotics applications (such as e.g. autonomous vehicles) [1]. Vision sensors facilitate object detection and localisation, which are crucial for navigation, obstacle avoidance, path planning, and performing specific tasks like manipulating objects or interacting with the environment [2], [3].

Typical frame-based cameras capture video sequences in grayscale or colour with specific spatial (e.g. 1280×720 pixels) and temporal (e.g. 60 frames per seconds) resolution. However, they can be challenging to apply in some circumstances

K. Jeziorek, P. Wzorek, K. Blachut and T. Kryjak are with the Embedded Vision Systems Group, Computer Vision Laboratory, Department of Automatic Control and Robotics, AGH University of Krakow, Poland. email: {kjeziorek,pwzorek,kblachut,tomasz.kryjak}@agh.edu.pl

A. Pinna is with the Sorbonne Université, CNRS, LIP6, F-75005 Paris, France. email: andrea.pinna@lip6.fr

This work was supported by the “Excellence initiative – research university” programme For AGH University of Kraków, the Polish National Science Centre projects 2024/53/N/ST6/04254 and 2024/53/N/ST6/04331 and Polish high-performance computing infrastructure PLGrid (HPC Center: ACK Cyfronet AGH – grant no. PLG/2023/016897).

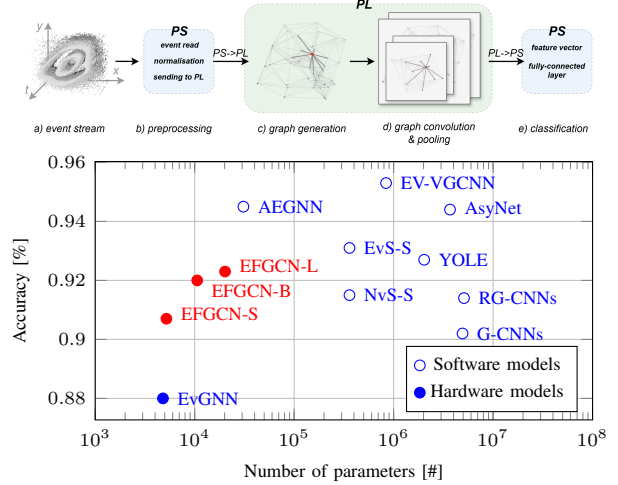


Fig. 1: Classification accuracy vs number of parameters of our EFGCN models on the N-Cars dataset compared with different asynchronous models.

because of issues such as motion blur during fast movements, high latency due to low frame rates, and difficulties in operating in uneven lighting conditions. These issues could be partially addressed by existing high-speed cameras, but these sensors are expensive and only work in good lighting conditions. Moreover, frame-based cameras generate large amounts of redundant data, which can be inefficient to process in real-time embedded systems.

In contrast, neuromorphic sensors, also known as event cameras or dynamic vision sensors (DVS), offer several advantages that address these limitations [4]. In a DVS, each pixel operates independently and asynchronously¹, detecting only changes in light intensity (not its level) and generating so-called ‘events’. Each event encodes the location (pixel coordinates), the timestamp (with microsecond precision), and the polarity (indicating increase or decrease in intensity). This approach results in lower average energy consumption, high temporal resolution, and reduced data redundancy, as the changes are only captured in place and time of their occurrence. Furthermore, since event generation is based on the logarithm of the brightness change, DVS has a high dynamic range maintaining satisfactory quality in environments with uneven illumination.

As highlighted above, event cameras have many advantages, especially for applications in dynamic environments for mobile

¹In the context of DVS, ‘asynchronicity’ is defined as the ability to generate or process events directly at the moment of an intensity change registered by a given pixel, without maintaining fixed time intervals.

robotics. However, the main problem is the efficient processing of the event stream. Computer vision methods developed over the last 60 years for frame cameras are not suitable for sparse spatio-temporal point clouds. Therefore, several approaches to this problem have been proposed. The simplest method is to project the event data onto a two-dimensional plane in order to create a pseudo-frame (often called event-frame), similar to the one obtained from a traditional camera [5]. This allows the almost direct application of classical methods and convolutional neural networks (CNNs) [6], [7]. However, this approach requires an aggregation of events over a given time interval resulting in an information loss (especially high temporal resolution), generation of redundant pixels, and higher latency. Therefore, recent research has focused on processing events in their original sparse form.

One recent approach is the use of graph neural networks (GNNs) through a generation of a graph representation. In such a structure, individual events are represented as vertices, while the edges connecting these vertices correspond to their local relationships. As a consequence, the data represented as a sparse cloud of vertices in spatio-temporal space can be processed efficiently with a graph neural network. In addition, recent research indicates that such graphs can be generated and updated asynchronously, thus not only reducing the number of operations for a single event [8]–[10], but also limiting the latency of data processing.

However, the biggest challenge remains the efficient processing of event data in a way that enables real-time² realisation of computer vision tasks with low latency, low energy consumption, and high throughput. It is important to emphasise that meeting these requirements is crucial for applications in mobile robotics. The literature includes research on hardware implementations of event-based vision algorithms, most commonly for embedded GPU platforms. Recently, FPGA (Field-Programmable Gate Array) systems have also gained increasing attention [11], [12], due to their low power consumption, high parallel processing capabilities, and flexibility enabled by hardware description languages. There is a growing collaboration between FPGA manufacturers and the DVS industry, driving advancements in event-based vision³.

In this work we propose **Event-based FPGA-accelerated Graph Convolutional Networks (EFGCNs)** – our strategy for efficient event data processing aimed at real-time and low-power mobile robotics applications. We can summarise our main contribution as follows:

- We present a series of optimisations for a GCN developed based on an analysis of the advantages and limitations of the target FPGA platform, extensive ablation studies, and evaluations for several event-based classification datasets.
- We present the first hardware implementation of a 3D MaxPool layer designed for event-data processing, which, by leveraging the temporal sparsity of event-based data, enables the deployment of larger network architectures and facilitates higher classification accuracy.

- We present one of the first end-to-end hardware modules for a GCN implemented on a SoC FPGA for real-time, continuous, sparse and asynchronous event data processing. This is the only implementation solely utilising elements of constant latency (no external memory) that supports each characteristic layer of a GCN.
- We achieve state-of-the-art performance among all hardware-implemented asynchronous approaches for multiple event-based classification datasets in terms of either model size or accuracy.

Our approach allowed us to significantly reduce the size of the model by up to 100 times, while limiting the accuracy loss to 2.2% and 2.9% for the N-Cars and N-Caltech101 datasets, compared to non-hardware state-of-the-art GCN methods. The proposed custom EFGCN hardware module implemented for heterogeneous ZCU104 System on Chip FPGA board achieves a processing throughput of up to 13.3 million events per second (MEPS) with a low latency of 4.39-9.31 ms. The prepared solution supports multiple configurations. Our approach offers strong scalability across various model sizes, input resolutions, and scene dynamics by leveraging highly parameterisable hardware modules. This design enables flexible adaptation of the system architecture to meet the specific requirements of a given application. These results present the potential of our approach for efficient real-time processing of DVS data in embedded systems. Both the software model and the hardware modules have been published as an open-source repository (<https://github.com/vision-agh/gcnn-dvs-fpga>).

The remainder of this paper is organised as follows. In Section II we present existing work on event data processing with an emphasis on FPGA-implemented approaches. Section III details our proposed method for hardware-aware design of graph convolutional network architectures for event data processing. A comprehensive description of the SoC FPGA implementation is provided in Section IV. In Section V we present the experiments conducted and ablation studies. The paper concludes with Sections VI and VII, where we present limitations, summarise our results and outline further work.

II. RELATED WORK

A. Event data processing

Currently, three main approaches are employed for event data processing. The first and most widely used approach involves **dense neural networks**, including convolutional neural networks (CNNs) [6], [7], [20]–[23] and vision transformers (ViTs) [24]–[26]. These methods deliver high-quality results and benefit from well-established techniques used for conventional image processing. However, they are not inherently designed for sparse and asynchronous events. To handle event data, these models first create dense representations like **event-frames** or **time-surfaces** [5], which introduces additional latency. In this approach also ‘empty’ pixels are processed, i.e. pixels without any events, which is inefficient in the case of sparse data. A compromise is achieved through asynchronous methods [22], [23], which update only local pixels, where events occur. Nevertheless, these models tend to have large memory footprints and high computational complexity,

²In computer vision, the precise definition of ‘real-time’ depends heavily on the application and sensor used. In this work, our aim is to process the event stream generated by the sensor in real time, without any significant delays.

³<https://www.prophesee.ai/event-based-metavision-amd-kria-starter-kit/>

TABLE I: Comparison of network models and hardware platforms used for event data processing by graph neural networks.

Work	Year	Network Model	Task	Platform
Sekikawa [13]	2019	PointNet	Semantic Segmentation and Ego-motion	CPU/GPU
Wang [14]	2019	PointNet/PointNet++	Gesture Recognition	GPU
Bi [15]	2019	SplineConv	Classification	Not mentioned
Mitrokhin [16]	2020	GraphConv	3D Classification	GPU
Li [8]	2021	GraphConv	Classification	CPU
Schaefer [9]	2022	SplineConv	Classification and Detection	GPU
Gehrig [10]	2022	SplineConv	Detection	GPU
Jeziorek [17]	2023	PointNetConv	Classification and Detection	GPU
Jeziorek [18]	2024	PointNetConv	Graph Generation and Detection	GPU/FPGA
Yang [19]	2024	PointNetConv	Classification	GPU/FPGA
Our	2025	PointNetConv	Classification	GPU/FPGA

while dense representations sacrifice high temporal resolution present in events.

The second approach utilises **spiking neural networks** (SNNs). They mimic the operation of brain neurons by accumulating membrane potential at each neuron and generating a spike once a certain threshold is exceeded. Since they are aligned with the event-based paradigm, SNNs can be directly applied to event cameras. However, the spiking mechanism inherent in SNNs is non-differentiable, making it difficult to apply the backpropagation approach for training [27]. Additionally, the results often fall short in quality, and the learning mechanisms require further research to enhance their performance [28]–[32].

The third and currently popular approach is to employ **graph convolutional networks** (GCNs) for the processing of event data. In this method, event data is represented as a spatio-temporal graph, with each event corresponding to a vertex connected to neighbouring vertices by edges. Table I compares various models and applications of GCNs for event data processing. Early work in this area demonstrated that GCNs significantly reduce the number of floating-point operations per event, due to their ability to maintain sparse data structures [15], [16], [33]. Moreover, later research demonstrated that they can be dynamically expanded by adding new events to the existing structure, with only local vertices that require updating [8]–[10], [34].

A notable contribution within this domain is the AEGNN framework [9], which introduced the concept of k-hop graph updates, achieving high-quality results with significantly reduced computational overhead compared to dense models. This approach has inspired further research [12], [17], [18], including our work. Moreover, since GCNs leverage standard backpropagation, this enables the training of larger models for complex tasks such as object detection [9], [10], [34]. Recent work [34] presents a hybrid system that integrates graph neural networks for event data with CNNs for frame data, highlighting the potential of GCNs for future applications. Overall, GCNs offer a balanced solution, combining the high-quality output of dense models with the efficiency of SNNs.

B. FPGA implementations

The advantages of FPGAs make them a suitable choice for processing event camera data. As a result, there has been a growing interest in combining event-based data processing

with FPGAs to develop energy-efficient vision systems. The most comprehensive review in this area was conducted in 2024 [11], which surveyed various FPGA-based solutions for event data processing.

Classical methods include HOTS [35] and PCA-RECT [36], which employ machine learning techniques like support vector machines (SVMs) combined with principal component analysis (PCA) for feature extraction. These methods require relatively low hardware resources, but their application to more complex tasks or larger datasets is limited. In contrast, FPGA-based event processing in AI can be divided into two subcategories: CNNs and SNNs.

SNN-based solutions are characterised by their low latency [37], [38], but the main drawback lies in the model sizes, as most SNN implementations use small input resolutions, typically around 32×32 or 64×64 pixels. As a result, their quality rarely approaches state-of-the-art performance. On the other hand, **CNN-based** solutions [39], [40] can achieve high performance but require significant hardware resources, exceeding the capacity of medium-sized FPGAs. This limits their applicability for edge devices and mobile robotics applications.

Besides the methods described, the first works addressing the topic of hardware implementation of GCNs on FPGAs have recently appeared. Our first work [17] emphasised the limitations of existing graph convolution methods. These studies revealed that most graph convolution layers require a large number of parameters and often depend on edge attributes, which increase the graph's size. The best-performing layer was found to be PointNetConv, which significantly reduces the number of parameters. It does not require edge attributes and improves the quality of the results.

A follow-up study [18] explored the hardware implementation of an efficient graph generation module for event data on the ZCU104 FPGA platform. This work introduced a matrix-based method for neighbour searches and demonstrated the advantages of using directed graphs, allowing asynchronous graph generation without the need of updating older vertices.

Finally, the most recent work [12], presents a complete system for event-based graph processing on FPGA. The authors adopted the same graph convolution method as in [17] and utilised directed graphs, similar to the approach in [18], [41]. They also evaluated different neighbourhood search patterns. However, a key limitation of this solution is the absence of pooling layers between convolutions, which

reduces the scalability of the network and increases the number of operations in subsequent layers.

In our work, we propose a solution to implement a graph convolutional neural network on an FPGA without relying on external memory, as its use increases energy consumption and introduces non-deterministic latency and bandwidth limitations. We demonstrate that this solution can be scaled to larger models and datasets through the use of pooling layers.

III. THE PROPOSED METHOD

Our research was motivated by the need to bridge the gap between the hardware implementation of GCNs and their application in event data processing. The goal was to develop a solution that maximises the use of information captured by event cameras, enabling accurate, real-time, event-by-event data processing with minimal latency, low computational load, lack of external memory usage and efficient resource utilisation. In this section, we outline the solutions and necessary modifications used for implementing a GCN on a SoC FPGA.

A. Event-Graph Construction

Event cameras are characterised by the ability to capture changes in brightness at the individual pixel level, which distinguishes them from traditional frame-based cameras. The operation of an event generation is governed by a threshold mechanism, which determines whether the change in light intensity for a specific pixel exceeds a predefined value. The outcome of this process is an event stream that can be described as a sequence of tuples $ev_i = (u_i, t_i, p_i)$, where $u_i = (x_i, y_i)$ indicates the pixel location at which the event was generated, t_i is the timestamp, and $p_i \in \{-1, 1\}$ denotes whether the change was negative or positive, respectively.

In the literature [9], [15], a **standard method** for generating a graph from events is to construct a spatio-temporal graph $\mathcal{G} = (\mathcal{V}, \mathcal{E})$, where each event ev_i is represented as a vertex $v_i \in \mathcal{V}$ with a position $\mathcal{P}_i = (u_i, t_i)$ and attribute $\mathcal{X}_i = (p_i)$. Subsequently, for each pair of vertices i and j , an edge $e_{ij} \in \mathcal{E}$ is generated, if their Euclidean distance d_{ij} represented as:

$$d_{i,j} = \sqrt{(x_i - x_j)^2 + (y_i - y_j)^2 + (t_i - t_j)^2} \quad (1)$$

is smaller than a predefined parameter R . To normalise the time dimension for better comparability with spatial coordinates, the timestamps t_i are scaled by a factor α , usually equal to the time window, resulting in $t_i^* = t_i \cdot \alpha$. Additionally, the number of edges is limited to D_{max} per vertex to avoid excessive edge generation.

However, directly searching for neighbouring vertices across the entire graph presents significant computational and memory challenges, especially in the context of hardware implementations, which would require using external memory, resulting in increased latency and energy consumption. Traversing all vertices in a graph of millions of events results in $O(n)$ complexity. Our objective is to minimise the number of searches per event to maintain real-time performance. Moreover, generating directed edges that support the continuous addition of new events without requiring updates to the

existing graph is crucial for efficient hardware processing, as discussed further in subsection III-B.

To address these challenges, we adopt the method proposed in [18], which optimises graph generation for hardware. For a comprehensive explanation of the method, refer to the original work. Below, we summarise the key steps of the approach.

Building on prior works [8], [9] and classical CNN-based models, the method begins by normalising both the spatial $u_i = (x_i, y_i)$ and temporal t_i coordinates to a common range β . The normalised coordinates are then discretised to integer values:

$$x_i^* = \left\lfloor \beta \cdot \frac{x_i}{W} \right\rfloor, \quad y_i^* = \left\lfloor \beta \cdot \frac{y_i}{H} \right\rfloor, \quad t_i^* = \left\lfloor \beta \cdot \frac{t_i}{T} \right\rfloor. \quad (2)$$

where (H, W) are the spatial dimensions of the input data, and T is the time window. This process maps the vertices into the set $\mathcal{V} \subset \mathbb{N}^3$, where each component ranges from 0 to β .

Neighbour searches are performed using a **neighbourhood matrix** (shortly NM), a two-dimensional matrix that corresponds to the normalised spatial resolution of the events. Each cell in the NM stores the timestamp and the polarity of the most recent event at a given spatial coordinate. For each new event ev_i , potential neighbours are searched among the pixels within a radius R of its position u_i^* . If the timestamp t_j^* of a neighbouring pixel u_j^* satisfies Eq. (1), a direct edge $e_{ij} \in \mathcal{E}$ is created and the timestamp in the matrix is consequently updated to t_j^* .

This approach allows for the initialisation of a fixed-size data structure $(\beta \times \beta)$, that stores information about previous events, limits the number of neighbour searches based on the parameter R , and enables the continuous processing of events while maintaining directed edges. The applied β parameter with spatial resolution (H, W) and time window T for different datasets used for the evaluation of our method are shown in Section V.

B. Graph Convolution

Among the various types of graph neural networks (GNNs), **graph convolutional networks** (GCNs) have become the most widely used model and form the foundation of our work. The core operation in GCNs is a convolution, which facilitates the efficient propagation of information between locally connected vertices. This enables updating vertex representations and extracting relevant features. Graph convolution generally involves three stages:

1. **Message Function** (ϕ): In the first stage, the message function ϕ operates on a vertex v_i and its neighbours $v_j \in \mathcal{N}(i)$, determining the information exchange between these vertices. The message function can utilise the vertex attributes $\mathcal{X}_i, \mathcal{X}_j$, their positions $\mathcal{P}_i, \mathcal{P}_j$, and edges \mathcal{E} .

2. **Aggregation Function** (\oplus): Next, the aggregation function \oplus combines the message values collected from all neighbouring vertices, producing a representative value that includes the information from the local neighbourhood of vertex v_i .

3. **Update Function** (γ): Finally, the update function γ adjusts the vertex attribute \mathcal{X}_i using the aggregated information.

The overall message passing process can be mathematically represented as Eq. (3).

$$\hat{\mathcal{X}}_i = \gamma \left(\bigoplus_{j \in \mathcal{N}(i)} \phi(\mathcal{X}_i, \mathcal{X}_j, \mathcal{P}_i, \mathcal{P}_j, \mathcal{E}) \right) \quad (3)$$

Here, both ϕ and γ are differentiable functions, typically implemented as multi-layer perceptrons (MLPs). The aggregation function \bigoplus can be a simple operator like sum or maximum.

As shown in Table I, several different convolutional layers are available and widely used, such as SplineConv [9], [10], [15], GraphConv [8], [16], or network architectures like PointNet and PointNet++ [13], [14]. However, these solutions often have high memory demands, which is not a major issue when using GPUs, but becomes critical in embedded implementations. The extensive memory utilisation by the convolutions has a potential to adversely impact the reduction in dimensionality or depth of the network, which leads to a loss in quality. Therefore, in our work, we focused on using the **PointNetConv**⁴ layer.

This choice was guided by the results of our prior research [17], where we achieved a significant reduction in model size and its inherent suitability for point cloud data. The PointNetConv layer is designed to efficiently process vertex features in 3D point clouds, implementing the transformation defined by Eq. (4):

$$\hat{\mathcal{X}}_i = \gamma \left(\max_{j \in \mathcal{N}(i)} \phi(\mathcal{X}_j, \mathcal{P}_j - \mathcal{P}_i) \right), \quad (4)$$

where ϕ is a function that processes the neighbour vertex attribute \mathcal{X}_j with the relative spatial coordinate $\mathcal{P}_j - \mathcal{P}_i$ and the max operator selects a representative attribute based on information received from the neighbours $\mathcal{N}(i)$. In our implementation, the message function ϕ is a simple linear transformation, mapping input features from dimension $in + 3$ to out , where the additional $+3$ accounts for the spatio-temporal dimensions of the events. To minimise complexity, we omit the update function γ , and in order to apply the BatchNorm merging [44], we used normalisation after ϕ function.

We investigated the effect of the convolution used on the model size and the results in Section V-B2.

Edge Directionality: In the case of graphs that are *bidirectional* or *directed against time*, each new event added to the graph can be connected to the neighbourhood $\mathcal{N}(i)$ of an existing vertex. This necessitates recalculating not only the attribute of the new event, but also the attributes of all vertices it is connected to. Such an update propagates further into the graph since each subsequent layer utilises information from more distant neighbours. This process, described in [9] as a **k-hop neighbourhood**, presents challenges for hardware implementations. Specifically, it requires storing information about previous vertices for each convolution and updating them continuously. In contrast, for graphs *directed with time*

new events are connected only to the nearest vertices, and only the new vertex needs updating. This significantly reduces the number of operations per event.

C. Graph MaxPool

Graph MaxPool is a technique used to reduce the number of vertices in a graph. It is particularly useful in deeper layers of neural networks, where the size of attributes can increase significantly. The technique involves partitioning the data space into uniform \mathcal{C}_k clusters of size $g_x \times g_y \times g_t$. For each of these non-empty clusters, a new vertex is selected whose attribute value corresponds to the maximum attribute value among all vertices in the cluster, as represented by Eq. (5).

$$\mathcal{X}_k = \max_{i \in \mathcal{C}_k} \mathcal{X}_i \quad (5)$$

Meanwhile, the position of the new vertex is determined as the average of the positions of all vertices in the cluster, as in Eq. (6).

$$\mathcal{P}_k = \frac{1}{|\mathcal{C}_k|} \sum_{i \in \mathcal{C}_k} \mathcal{P}_i \quad (6)$$

In this process, connections that link vertices from different clusters are merged into a single edge between new points, eliminating redundant connections and those internal to the groupings.

In the works [9], [10], the MaxPool operation is performed two-dimensionally with respect to space, meaning each cluster has a g_t parameter set to the maximum value. As a result, for a given spatial range $g_x \times g_y$, there can be only one output vertex. This was motivated by computational reduction due to a significant decrease in the number of vertices. However, there are two key issues with this approach. The first is the continuous change in the spatial structure of the graph after pooling, as with each new event ev_i the position \mathcal{P}_k is modified according to Eq. (6). The second issue, highlighted by the authors in [10], is that this operation can cause bidirectional edges between output nodes. Both effects significantly impact the continuous updating of the graph itself as well as the recalculation of vertex attributes, which in case of FPGA results in a constant need to read, recompute, and write data.

To address this, we propose two modifications to this method to enable its hardware implementation. The first modification is to apply 3D pooling, where the cluster size is set to the same value for each dimension, so $g_x = g_y = g_t = g$. The result is a larger number of vertices compared to the 2D method, but the pooling operation is divided into time intervals, which negates the need to update vertices in the temporally older parts of the graph. The second modification is to scale down the vertex positions according to the cluster size, so that each position value \mathcal{P}_k is divided by the parameter g . This ensures that the edges in the output graph remain directed with time and reduces resource consumption on the FPGA.

Our analysis in Section V-B1 shows that using 3D pooling positively affects the qualitative performance. Also, scaling the graph down causes a significant reduction in both memory and logic resources (see Sections IV-C and IV-D).

⁴The implementation of the PointNetConv layer presented here is based on its implementation in the PyTorch Geometric library [42], which is based on the work [43].

IV. HARDWARE IMPLEMENTATION

After extensive ablation studies in software (Section V-B), we developed a set of hardware modules for processing an event stream using graph convolutional neural networks. Our custom architecture implemented in SystemVerilog was simulated for consistency with the software model and evaluated across multiple configurations on the Zynq UltraScale+ MPSoC ZCU104 Evaluation Kit (featuring the XCZU7EV-2FFVC1156 chip).

The hardware architecture was designed as a pipeline of modules implementing successive layers of a graph convolutional network that process data in a completely parallel manner – each layer can process data simultaneously, as long as its input data is available (Fig. 2). During inference, only internal memory resources are used, ensuring constant latency. The system consists of two parts – asynchronous (operating in an event-by-event manner) and synchronous, where operations are performed on sub-graphs. The toolchain can process sequence of events of any length continuously, generating a prediction at the output for data recorded during the last TIME_WINDOW (duration of a single sample of event data sufficient to perform the classification – in described configurations we support windows of 50 ms and 100 ms), but 4 times as fast (features available on system’s output every $\text{TIME_WINDOW}/4$).

The system assumes the use of a heterogenous SoC FPGA platform, where feature extraction is implemented in the programmable logic (PL) and the network head is performed in the processing system (PS). The operating frequency of 200 MHz was selected based on experimental evaluation to balance latency and timing requirements. In the following sections, we present the functional description of each hardware module, preserving their order in the system pipeline.

A. Graph generation ($u_generate_graph$)

For testing purposes, in the designed system consecutive events are read by the processor from an SD card and then transmitted to the programmable logic in such a way as to maintain the intervals between the events, corresponding to their timestamps (emulating the actual output of the DVS). We also successfully evaluated the continuous processing of data read directly from DVS integrated with the PL.

The events are then normalised in the FPGA (Eq. (2)) – the coordinate values x, y and the timestamp t are scaled to $0-\beta$ (graph size) range. Currently, we support graphs sizes of $128 \times 128 \times 128$ and $256 \times 256 \times 256$. The polarisation value is encoded as a single bit. The normalised events are written into a FIFO queue implemented with BlockRAM to be then read by the following modules. This buffering mechanism ensures correct processing when the dynamics of the observed scene exceed the system’s bandwidth.

The subsequent events read from the FIFO are used to update the graph representation (Section III-A). For this purpose, it is necessary to determine the list of neighbours for the currently processed vertex. With the use of a directed graph, the data in the first part of the system is processed event-by-event – the registration of a new event does not require up-

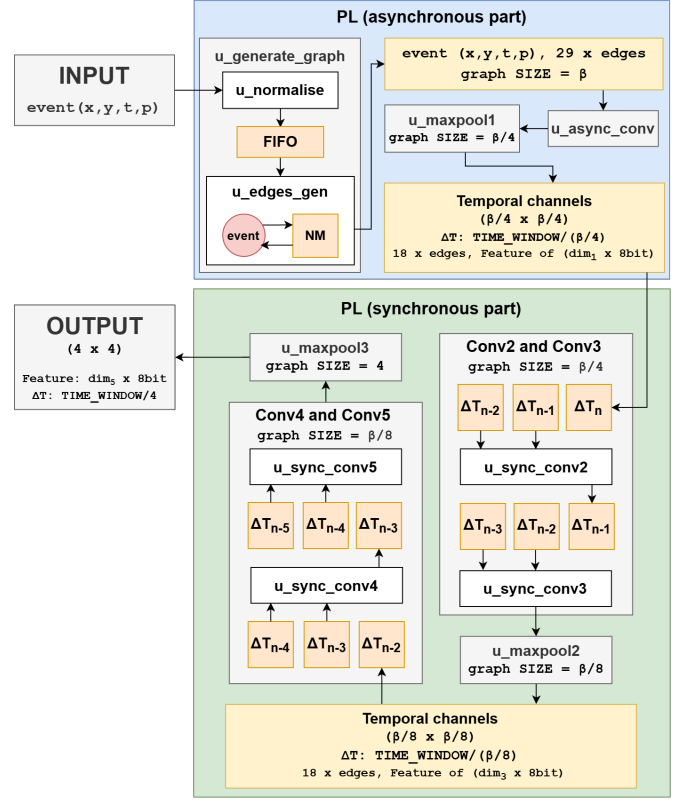


Fig. 2: Schematic of the EFGCN network hardware modules with the asynchronous part marked with blue and the synchronous with green. The orange modules represent integrated memory, while the characteristics of data transferred between the selected modules are highlighted with yellow blocks. The number of features for particular graph convolution layer $\text{dim}_1\text{-dim}_5$ depends on the model (Small, Base or Large). We support $\beta = 128$ and $\beta = 256$ configurations.

dating previously processed ones. The **neighbourhood matrix** NM (Section III-A) is implemented as a two-port BlockRAM memory of $\beta \times \beta$ depth and width of $\beta+2$ (storing the timestamp of the last recorded event for a particular pixel, its polarity and is_empty flag). For each event read from the FIFO, the edge candidates are read from the NM – 29 surrounding values (for $R = 3$). For each read, the semi-sphere condition is checked (Eq. (1)). Next, the currently processed event is written to the NM . This operation, due to the use of dual-port memories, requires 15 READ operations on one of the ports, and 14 READ operations and one WRITE operation on the other.

The latency of 15 clock cycles for a single event is a computational bottleneck of the proposed system. It can be determined that, with a 200 MHz clock, the throughput of the proposed system is 13.3 MEPS (million events per second), which significantly exceeds the values observed for real event stream data in the utilised datasets (1.35 MEPS for N-Caltech101, 0.59 MEPS for N-Cars, 0.34 MEPS for CIFAR10-DVS, and 0.063 MEPS for MNIST-DVS).

Once the NM analysis is complete, the module outputs pairs of events $(x, y, t, \text{and polarity})$, and a vector describing

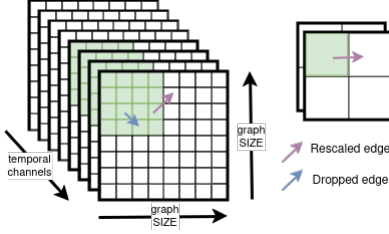


Fig. 3: Operation of the 3D MaxPool layer. The green area refers to the pooling region before and after the max.

their edges (including polarity of connected events).

B. Asynchronous convolution (u_async_conv)

Successive pairs of events and their edges appear at the first convolution module's (Section III-B) input asynchronously with preserved order – no more frequently than once every 15 clock cycles, but with an unknown time span (depending on the dynamics of the observed scene). For each processed vertex, the graph convolution (implementation of Eq. (4)) requires performing maximum of 30 multiplications – one for its own feature map (self-loop) and one for the feature map of each neighbouring vertex connected by an edge (a maximum of 29). The input feature map consists of four components: polarisation and the positional difference between connected vertices (for the self-loop, this is $(0, 0, 0)$). No extra memory is required, since the described initial convolution process only the values that are already present in the module's input.

The implementation of the linear function ϕ (Eq. (4)) utilises two parallel modules for matrix multiplication, which are realised in LUT logic resources. For the first convolutional layer, all elements of the output vector are computed in parallel – therefore, the processing time for a vertex-edge pair is 15 clock cycles. For each resulting value (after adding the bias), a requantisation process is required. It consists of scaling (using DSP and bit-shifting) followed by the addition of a constant `ZERO_POINT`. The resulting vectors for each edge (and self-loop) are compared with an element-wise maximum operation (taking into account layer-specific minimum values – ReLU activation). This generates the final feature map vector, which is propagated to subsequent model layers. The output of the module is the currently processed event, a list of its edges and a vector of its features.

C. 3D MaxPool ($u_maxpool$)

Immediately following the first convolution, a 3D MaxPool operation (Section III-C) with a $4 \times 4 \times 4$ kernel is applied. Its purpose is to scale the graph in each of the three dimensions – x, y, and time – by replacing the input events within $4 \times 4 \times 4$ regions with a single output vertex. Consequently, the graph of $SIZE$ (for the input graph $SIZE = \beta$) is replaced for subsequent layers with a graph of $SIZE/4$. The output feature vectors are the results of an element-wise maximum operation (Eq. (5)); visualised on Fig. 3) applied to all inputs within a given region. This operation leads to the following:

- The number of processed vertices for subsequent layers in the network model will be reduced 16 times, leading to a significant decrease in the required memory resources.
- The number of edges will also be reduced. After 4×4 clustering, the maximum positional difference between connected vertices is reduced to $R = 1$, and their number is reduced to 17. As a consequence, the maximum number of multiplications required for graph convolution in subsequent layers is reduced (from 30 to 18).
- The processing order of events will be disrupted. Scaling the graph not only among the x and y coordinates, but also in the time plane, forces data accumulation within specific intervals. Subsequent layers can only process data once the accumulation is complete.

The hardware module of *Relaxing MaxPool* operates on the BlockRAM *feature memory* with a depth of $(SIZE/4)^2$, which is addressed using x and y coordinates. Subsequent events are assigned to one of its cells, where the feature map is stored along with an updated list of its edges. A single read and write operation of a given cell allows the execution of the element-wise $\max()$ when more than one event is assigned to it. Event accumulation is performed within a time unit:

$$\Delta T = \frac{TIME_WINDOW}{(SIZE/4)}. \quad (7)$$

As a result, the *feature memory* contains the complete feature map after a ΔT period defined by Eq. (7), and only then can it be processed by subsequent layers. The disruption of event order forces a change in the data processing method in the next part of the model (referred to as 'synchronous') – instead of event-by-event processing, two-dimensional feature maps called *temporal channels* are processed, representing all events that occurred within a given ΔT .

A significant advantage of using the 3D MaxPool module is the ability to precisely determine the required throughput for each subsequent layer in the synchronous part of the system. Based on this value, an appropriate computation strategy is chosen to ensure that as many operations as possible can be executed sequentially. In summary, the 3D MaxPool not only reduces memory usage but also the consumption of LUT resources for subsequent multiplications.

D. Synchronous Graph Convolution (u_sync_conv)

To process the entire *temporal channel*, it is necessary to compute the output of the linear function ϕ (Eq. (4)). For each element, the system must read the feature maps of the currently processed vertex as well as all vertices connected to it by an edge, resulting in a maximum of 18 memory accesses. Notably, eight of these potential edges connect vertices within the same ΔT , while the remaining nine connect to neighbouring vertices from the previous ΔT ($R = 1$ along the temporal axis as well). Executing this convolution requires access to the last two *temporal channels*, a constraint that was taken into account when designing the 'feature memory' mechanism (Fig. 5).

The computation of the linear function ϕ for a single vector x_i consists of the following (Fig. 4):

- The vector x_i is constructed by aggregating an n-element feature vector (retrieved from 'feature memory') and

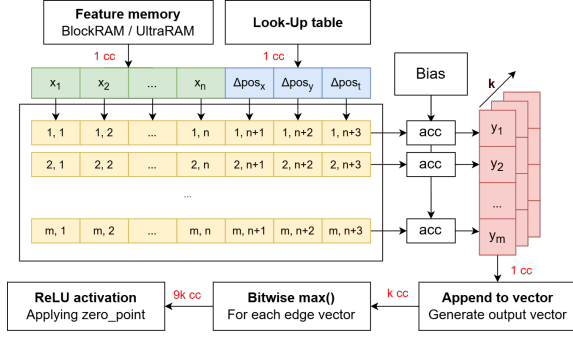


Fig. 4: The graph convolution module in the synchronous part of the system. The input vector, composed of features retrieved from memory (green) and position differences (blue), is processed by the multiplier matrix (yellow). The resulting vector (red) is generated through an append operation in k steps, with m elements each.

three position difference values (Eq. (4) – \mathcal{P}). The position differences are obtained from a Look-Up Table (LUT) based on the coordinate differences between vertices connected by an edge.

- Each element of the output vector $\phi(x_i)$ is computed by multiplying x_i by a weight vector. Depending on the required module throughput (determined by ΔT), the number of parallel vector multipliers (m) can be adjusted. The more multipliers are used, the higher the resource consumption. Therefore, the smallest possible value of m to ensure that the required throughput is maintained without exceeding resource constraints is selected.
- For each iteration (i.e. in each clock cycle), m elements of the output feature vector are determined. This process is repeated k times for a single input vector to obtain the $\phi(x_i)$ of dimensions $\dim = m \times k$.

With the required access to two preceding *temporal channels*, which are stored in independent ‘feature memory’ units, the system processes two vectors simultaneously by default. The convolution result for a given vertex is determined as the outcome of the bitwise max operation applied to all $\phi(x_i)$ vectors. The number of clock cycles (CC) required for this computation can be expressed as:

$$CC_{vertex} = 9 \times \frac{\dim}{m}, \quad (8)$$

where \dim represents the size of the output feature map, and m denotes the number of parallel multipliers used. In summary, the processing of an entire *temporal channel* takes:

$$CC_t = CC_{vertex} \times SIZE \times SIZE \quad (9)$$

where $SIZE$ represents the current size of the processed graph, which decreases after each successive MaxPool.

The strategy for reducing LUT resource utilisation involves selecting the maximum number of parallel multipliers m so that ΔT_{cc} (in clock cycles) satisfies Eq. (10).

$$\Delta T_{cc} \geq 9 \times \frac{\dim}{m} \times SIZE \times SIZE \quad (10)$$

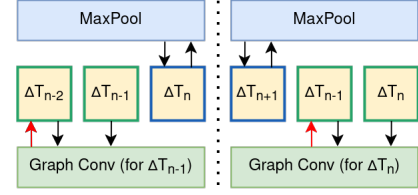


Fig. 5: The memory switching method – memory blocks are represented as yellow squares, while arrows indicate memory writes and reads. The red colour denotes memory reset.

In the synchronous part of the system, each graph convolutional layer can employ a different multiplication strategy (for decreasing $SIZE$ with each MaxPool).

E. Memory management

For GCN inference, it is necessary to store intermediate feature maps (in the synchronous part) as well as weights. In the proposed hardware module, only internal memory resources (BlockRAM and UltraRAM) are utilised – access to DDR memory is not required. To minimise memory resource usage, a memory-sharing mechanism has been implemented between successive layers (Fig. 5).

Each module implementing the *feature memory* consists of three independent memory blocks (implemented with BlockRAM or UltraRAM, depending on the feature vector size). While the preceding layer (e.g. MaxPool) writes data to one of these memory blocks generating a *temporal channel* for ΔT_n , the other two (storing data for ΔT_{n-1} and ΔT_{n-2} , respectively) are used by the next layer. Once convolution processing for an entire *temporal channel* is completed, the oldest memory block (corresponding to ΔT_{n-2}) is reset. An appropriate multiplication strategy ensures that the graph convolutional layer completes processing before the next *temporal channel* is ready. At that point, memory switching occurs so that new data is stored in the recently cleared memory block.

Weight matrices are stored in distributed RAM for the first (asynchronous) convolutional layer due to the requirement for simultaneous access and the relatively small size. In the synchronous part of the network, the weight matrices are stored in BlockRAM. However, the memory utilised for this purpose represents only a small portion of the overall usage.

F. Hardware module's output

Regardless of the chosen configuration of the GCN architecture, the processed graph at the output of the reconfigurable part of the system (after the sequence of MaxPool layers and graph convolution) has a size of $SIZE = 4$. As a result, successive *temporal channels* are transmitted to the software part of the heterogeneous system every $TIME_WINDOW/4$ ms. The final feature map is used as input to the linear layer implemented in the PS to determine the classification results. We implemented the HEAD of the network in the PS to increase the versatility of the proposed architecture – the same hardware module for feature extraction can be used for different computer vision tasks (while it could be implemented

TABLE II: Details of statistics and parameters used during graph generation for the event datasets used, including N-Cars (N-C), N-Caltech101 (N-Cal), CIFAR10-DVS (C-DVS) and MNIST-DVS (M-DVS).

Datasets	N-C [45]	N-Cal [46]	C-DVS [47]	M-DVS [48]
Samples	24029	8246	10000	30000
Classes	2	100	10	10
Duration	100 ms	300 ms	1280 ms	2-3 s
Resolution	120×100	240×180	128×128	128×128
Normalisation β	128	256	128	128
Time window	100 ms	50 ms	100 ms	100 ms

in reconfigurable logic, with relaxed throughput requirements, this is not necessary). In the case of continuous event data processing, predictions can be generated every $\text{TIME_WINDOW}/4$ ms, with each prediction taking into account the most recent TIME_WINDOW ms of data.

V. EXPERIMENTS

A. Setup

1) *Datasets*: In our experiments, we focused on the object classification from events. We selected four commonly used datasets including N-Cars [45], N-Caltech101 [46], CIFAR10-DVS [47], and MNIST-DVS [48]. The details about the dataset statistics and the parameters used during graph generation are summarised in Table II. For the N-Caltech101 dataset, due to the larger resolution and dynamics, the normalisation parameter β is set to 256 and TIME_WINDOW to 50 ms.

2) *Model details*: For the software implementation of the models, the Torch framework [49] was used along with the PyTorch Geometric library [42]. All experiments were performed on our three EFGCN models: Small, Base, and Large. Each model consists of 5 convolutional layers and two MaxPool layers. A PoolOut layer was used at the end of each model, which is a simple 2D MaxPool and a single MLP layer for classification.

Each model was implemented on the heterogeneous ZCU104 platform in two configurations: $\beta = 128$ with $\text{TIME_WINDOW} = 100$ ms and $\beta = 256$ with $\text{TIME_WINDOW} = 50$ ms. For a 200 MHz clock, both configurations meet the timing requirements. Simulation results confirmed the consistency of the hardware module with the software model and the previously estimated throughput of 13.3 MEPS. For the $\beta = 128$ configuration, computing all output feature map elements independently for each convolution (i.e. with $m = 1$) satisfies the required throughput. However, for larger graphs and smaller time windows, parallelisation of certain multiplications is necessary. The number of parallel vector multipliers required for each configuration is presented in Table III (details are available in the supplementary material).

3) *Training details*: In all experiments, the Adam optimiser [50] was used along with the ExponentialLR scheduler. Each model was trained for 100 epochs, and for model quantisation the QAT technique was applied for additional 50 epochs. During training, we used data augmentation in the form of event flipping along the X-axis and event rotation by a random angle with respect to the time axis.

TABLE III: The number of parallel vector multipliers m required to meet the throughput requirements for each model (with a $\beta = 256$ and a TIME_WINDOW of 50 ms).

Model	Output \dim				Parallel multiplications m			
	Conv2	Conv3	Conv4	Conv5	Conv2	Conv3	Conv4	Conv5
EFGCN-S	32	32	32	32	8	8	1	1
EFGCN-B	32	32	64	64	8	8	2	2
EFGCN-L	32	64	64	128	8	16	2	4

TABLE IV: Ablation studies on MaxPool modifications on accuracy on the N-Cars dataset show that the incorporation of 3D MaxPool enhances overall performance. However, dividing the position component has been observed to slightly degrade the results.

2D MaxPool	3D MaxPool	Average \mathcal{P}	Divide \mathcal{P}	Accuracy
				0.887
✓		✓		0.918
✓			✓	0.917
	✓	✓		0.922
	✓		✓	0.920

B. Ablation studies

Our ablation studies focus on three key elements, which are the number of parameters (memory usage), FLOPs (number of floating-point operations) and classification accuracy (performance). If not specified, the Base model and N-Cars dataset were used as a basis. As a comparison, we used two recent works: EvGNN [12] which shows a hardware implementation of GCNs for event cameras, and AEGNN [9] which was the inspiration for EvGNN and our works.

1) *Impact of MaxPool modifications*: We start our analysis with the impact on the quality results of the modifications we applied to the pooling layers, which are shown in Table IV. In [9], a 2D pooling method with an *average* position was introduced, while in [12], the pooling layer was entirely omitted. Our results show that excluding the MaxPool significantly degrades performance, primarily due to its role in data generalisation in subsequent stages of the model, leading to improved outcomes. Additionally, we observe that adopting a 3D pooling operation enhances accuracy by approximately 0.3-0.4% compared to the 2D pooling method. In contrast, the use of *divide* position has a slight negative impact, reducing accuracy by around 0.1-0.2%.

Next, we compared the impact of using MaxPool layers and their absence in terms of the graph size and required operations. Figure 6 illustrates a comparison of the total number of FLOPs performed by individual convolutions and the reduction in the number of vertices and edges in the graph. It can be observed that the number of FLOPs is closely correlated with the number of edges, primarily due to the operation of the PointNetConv layer, which applies a linear transformation to each connection. Without the pooling operation, neither the number of edges nor vertices decreases, leading to 50 times more operations in subsequent convolutions, showing a major drawback of the solution in [12].

These results underscore the critical role of MaxPool layers, not only for improving qualitative outcomes, but also for enhancing computational efficiency. Our proposed 3D pooling

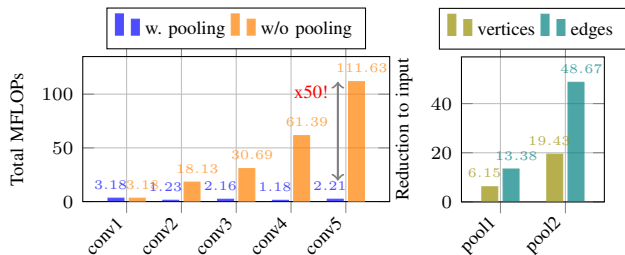


Fig. 6: Comparison of the number of operations per second (left) and number of vertices and edges (right) with and without the use of MaxPool layers. The use of pooling significantly reduces both the number of operations and graph complexity.

TABLE V: Comparison of our methods with other architectures in terms of the number of parameters and accuracy for the N-Cars dataset. The results demonstrate that our solution has a positive impact in both aspects.

Model	Accuracy	Num. of parameters
AEGNN	0.893	30.4k
EvGNN	0.880	4.8k
O-AEGNN	0.898	5.0k
O-EvGNN	0.891	4.2k

method maintains performance levels comparable to those presented in [9] and significantly outperforms the approach in [12] in all aspects.

2) **Impact of all modifications:** To evaluate the impact of our convolution and graph generation modules along with the previously described MaxPool layers, we compared them with two state-of-the-art models in terms of size and performance. The AEGNN [9] model consists of 7 SplineConv layers [51] with one 2D MaxPool layer and two skip-connections, while the EvGNN [12] model consists of 4 convolutional layers without any MaxPool layer.

To gain more comprehensive understanding of how our methods influence model size and performance, we introduced modified versions of both architectures: O-AEGNN and O-EvGNN. In these models, we replaced the original graph generation, convolutional, and MaxPool layers with our custom modules. Additionally, in the O-EvGNN model, we incorporated two MaxPool layers placed after the first and third convolutional layers.

The results presented in Table V demonstrate the impact of the proposed modifications. For the AEGNN, integrating our modules significantly reduces the number of parameters, which can be attributed to the complexity of the original SplineConv layers, as discussed in [17]. In the case of the EvGNN models, the number of parameters is slightly smaller, reflecting the reduced number of feature vectors returned by the feature extractor. In both cases, our modifications lead to improvements in qualitative results, highlighting the advantages of our approach.

3) **Quantisation precision:** Although our hardware implementation was designed for 8-bit precision, it is crucial to explore the potential for quantising to lower bit precisions with Quantisation Aware Training (QAT). In Figure 7, we compared

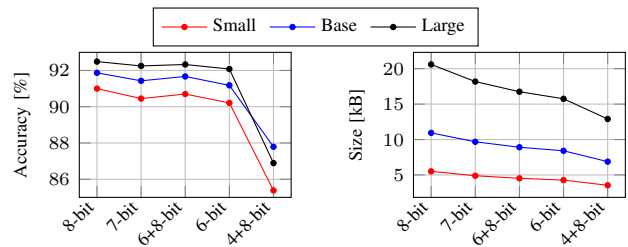


Fig. 7: Comparison of models accuracy and size for different precisions. The results indicate that quantisation to 6 bits still enables relatively high accuracy for each model.

the qualitative results and model sizes for different bit-widths. We analysed standard 8-bit, 7-bit, and 6-bit quantisation, and experimented with mixed precision quantisation, where part of the feature extraction was quantised to lower bit-widths (6/4 bits) while keeping the classifier at 8-bit.

The results show that 6-bit quantisation, which reduces the model size by approximately 23%, has a small impact on model quality, where in the case of 4-bit quantisation there is a significant degradation in performance. It is worth noting that using 6-bit feature extractor with 8-bit classifier gives better results and size reduction of about 8% compared to full 7-bit quantisation. In our models, where feature extraction part is implemented in the PL and the classifier in the PS, this modification could be crucial for deploying complex models.

C. Comparison with other works

In this section, we compared our three models (small, base and large) with state-of-the-art based on the N-Cars, N-Caltech101, CIFAR10-DVS, and MNIST-DVS datasets. The results in terms of accuracy, FLOPs per event, and network size are presented in Table VI. We primarily selected methods that use graph-based event representations [8], [9], [12], [15], but also included other asynchronous methods, such as SNNs [28] and dense neural networks [20], [23].

A few conclusions can be drawn from the results. First, our models clearly outperform all solutions in terms of the number of FLOPs per event, where in the case of YOLE the difference is more than 1000 times, while for the EvGNN, which is smaller than our Base model, it achieves larger FLOPs per event. This shows the significant advantage of GCN methods over dense methods in terms of computational complexity and our 3D MaxPool over other GCN approaches. Second, our models are among the smallest in terms of number of parameters, with the exception of the EvGNN model, which achieves almost the worst result for the N-Cars dataset. In the case of the AEGNN model, the difference in size reaches up to 100 times in the number of parameters.

Qualitatively, our Small model outperforms the G-CNNs, HATS and YOLE models on individual datasets. On the other hand, our Large model performs better than NvS-S, while it comes close to YOLE for the N-Cars, AEGNN and HATS for the N-Caltech101 and EvS-S for the MNIST-DVS. However, it should be noted that some graph methods use large values of the radius for edge generation (e.g. 5 in AEGNN for the

TABLE VI: Comparison with other methods of object classification for Float32 models. The results show that our models are among the smallest in terms of the number of parameters and exhibit the lowest computational complexity per event, while achieving results comparable to the state-of-the-art. In parenthesis there are values obtained from the open source code.

Model	Repr.	Async.	N-Cars		N-Caltech101		CIFAR10-DVS		MNIST-DVS		# Param. ↓
			Acc. ↑	MFLOPs/ev ↓	Acc. ↑	MFLOPs/ev ↓	Acc. ↑	MFLOPs/ev ↓	Acc. ↑	MFLOPs/ev ↓	
H-First [28]	Spike	✓	0.561	-	0.054	-	-	-	-	-	-
HATS [45]	Time-Surface	✓	0.902	0.03	0.642	4.3	0.524	0.18	0.984	0.18	-
YOLO [23]	Voxel-Grid	✓	0.927	328.16	0.702	3659	-	-	0.961	-	2.03 M
AsyNet [20]	Voxel-Grid	✓	0.944	21.5	0.745	202	0.663	103	0.994	112	3.69 M
G-CNNs [15]	Graph	✗	0.902	-	0.630	-	0.515	-	0.974	-	4.93 M
RG-CNNs [15]	Graph	✗	0.914	-	0.657	-	0.540	-	0.986	-	5.10 M
NvS-S [8]	Graph	✓	0.915	5.2	0.670	7.8	0.602	22.8	0.986	10.1	0.36 - 1.16 M
EvS-S [8]	Graph	✓	0.931	6.1	0.761	11.5	0.680	33.2	0.991	15.2	0.36 - 1.16 M
AEgNN [9]	Graph	✓	0.945 (0.893)	0.47	0.668 (0.643)	7.31	-	-	-	-	0.03 - 20.4 M
EvGNN [12]	Graph	✓	0.880	0.063	-	-	-	-	-	-	4.8 k
EFGCN-S	Graph	✓	0.907	0.032	0.623	0.004	0.571	0.011	0.964	0.006	5.2 - 55.5 k
EFGCN-B	Graph	✓	0.920	0.060	0.631	0.008	0.588	0.022	0.978	0.012	10.6 - 111.0 k
EFGCN-L	Graph	✓	0.923	0.111	0.639	0.015	0.613	0.040	0.983	0.022	20.2 - 220.9 k

TABLE VII: Comparison of the EFGCN with the SOTA in terms of resource utilisation, accuracy and latency on SoC FPGAs.

Model	Graph size	Time window	Utilisation					Accuracy [%]				Latency		
			LUT	FF	BlockRAM	UltraRAM	DSP	N-Cars	N-Caltech101	CIFAR	MNIST	PL [ms]	PL+PS [ms]	per ev. [μ s]
EFGCN-S	128	100 ms	43553	15292	121.5	0	90	91.0	-	57.4	98.7	3.78	4.39	6.56
EFGCN-B	128	100 ms	53517	18798	162	0	90	91.9	-	59.1	97.9	4.62	5.77	9.44
EFGCN-L	128	100 ms	65901	24622	211.5	0	90	92.5	-	61.5	98.5	7.03	9.31	13.76
EFGCN-S	256	50 ms	112670	24087	149	12	172	-	62.8	-	-	4.42	5.12	4.02
EFGCN-B	256	50 ms	139382	29401	187.5	12	184	-	63.2	-	-	4.43	5.77	4.04
EFGCN-L	256	50 ms	142773	38882	240	12	1364	-	64.1	-	-	4.43	7.11	4.04
EvGNN [12]	120 × 100	-	30908	24083	15	48	228	87.8	-	-	-	-	-	16
ESDA [40]	180 × 240	-	154000	115000	1278	0	1792	-	72.4	-	-	3.09	-	-

N-Caltech101 and 5 in NvS-S/EvS-S for all datasets), which has a key impact on the quality of the results, as we have analysed in detail in the supplementary materials.

D. Comparison with other hardware implementations

In Table VII, we present a comparison with the solutions proposed in the literature on event-based object classification systems implemented in FPGAs in terms of resource utilisation, model accuracy after quantisation and latency.

We considered each of the EFGCN network models (Small, Base, Large) for hardware implementation. For models with the $\beta = 256$ configuration, part of the multiplications was realised using DSPs rather than LUTs to reduce the usage of the latter (hence the variable DSP usage).

The latency of the PL (graph generation, feature extraction) is defined as the time between the registration of the last event in a given sequence and the reception of the final feature map in the PS. The total latency, including the additional processing of the network’s HEAD, is defined as PL+PS latency.

The proposed EFGCN enables predictions to be generated every 25 ms with latency of 4.39-9.31 ms (for the configuration with `TIME_WINDOW = 100 ms`), or every 12.5 ms with a latency of 5.12-7.11 ms (for the configuration with `TIME_WINDOW = 50 ms`). Moreover, the use of elements with fixed latency only (no access to external memory for convolutional layers) allowed for the determination of a constant system throughput of up to 13.3 MEPS, the value not achievable for alternative solutions.

The analysis of the achieved latency leads to some interesting conclusions. Firstly, for models with `TIME_WINDOW = 100 ms` configuration, increasing the model size leads to

higher latency, because for each convolution we set a number of parallel multipliers $m = 1$. As the feature map sizes increase, the number of necessary multiplications grows, and consequently, the time required to perform them increases. This issue does not occur in `TIME_WINDOW = 50 ms` configuration. Regardless of the feature map sizes, the measured latency remains similar – close to 4.43 ms. With more stringent throughput requirements, different multiplication strategies were adopted for each layer. The larger the number of elements in the feature map, the more parallel multipliers were used. As a result, the amount of utilised resources increases, but the latency remains constant. Based on these observations, it can be concluded that in the proposed system, latency and resource usage are correlated, and their appropriate selection should be motivated by the specific requirements set for the given application. The obtained latency can be improved with increased LUT utilisation.

With the limited number of experiments conducted by alternative solutions, direct comparison is only possible using the N-Cars and N-Caltech101 datasets. For the **N-Cars** dataset, our method achieves the highest accuracy scores among all those proposed in the literature for each GCN model (Small, Base, and Large). Moreover, our Small model achieves a 3.2% higher accuracy than EvGNN [12], with 41% higher LUT utilisation, while simultaneously reducing FF resources by 36%, DSPs by 60%, and internal memory resources by 70% (estimation based on a 32 kb capacity for BlockRAM and 288 kb for UltraRAM).

In [12], the system latency for entire sequences was not measured, and instead, latency per event was used as the metric. To enable a direct comparison of these methods, Table

VII also presents the per-event latency calculated as the sum of the delays of the individual hardware modules. However, it should be noted that this metric is not perfect for our method, as it does not reflect its operational nature (primarily due to the synchronisation of computations and feature map buffering induced by the MaxPool layers – Section IV).

The key difference between EvGNN and EFGCN is the three-dimensional MaxPool mechanism we employed, which enables the exploitation of the temporal sparsity of the data. The system described in [12] achieves low latency by processing events asynchronously for the entire network. However, it should be emphasised that in doing so, the authors opted out of data scaling between convolutional layers, which leads to a significant increase in computational complexity (Section IV). To maintain low latency in the system, feature maps of small sizes (maximum of 32 elements) were used, and a matrix multiplication strategy based on a high level of parallelism (MAC engine per output channel) was adopted.

At the same time, by using 3D MaxPool, EFGCN offers significantly better scalability through efficient computation, achieving higher classification accuracy with the use of fewer resources. The ability to configure the level of parallelism in matrix multiplication allows for adjusting the achieved latency to the specific computer vision problem. In the case of EvGNN, on the other hand, increasing the size of individual feature maps or the number of layers significantly impacts both latency and resource usage. In summary, by employing 3D MaxPool, the EFGCN model is more scalable for data with higher resolution and greater dynamics. It should also be emphasised that the system described in [12] utilises external DDR memory resources, which leads to variable latency and significantly increases energy consumption (access to DRAM accounts for over 50% of the energy consumption in the EvGNN system).

In the case of **N-Caltech101**, our module allows for classification with accuracy ranging from 62.8% to 64.1%. The system proposed in [40], which utilises sparse convolutional neural networks, achieves higher accuracy. However, the utilisation of this method is higher across all considered resources. The main issue is the very high usage of internal memory resources (between 5.3 and 8.5 times higher compared to the individual EFGCN models). Implementing ESDA for the ZCU104 platform considered in this paper would not be feasible due to the usage of FF, DSP, and BlockRAM resources exceeding the available number of elements (in the case of BlockRAMs – 4 times). At the same time, given the motivation related to the use of event-based cameras for mobile robotics, limiting resource utilisation is one of our priorities.

While the latency of 3.09 ms achieved in [40] is nominally lower than the one achieved by EFGCN, it is important to consider the differences in operation. Due to the use of two-dimensional event-frame representations, systems utilising convolutional neural networks require prior data buffering and frame generation. In contrast, our system processes events directly as soon as they are registered. EFGCN allows for predictions 4 times more frequently than the `TIME_WINDOW` value, thus providing greater throughput than a solution requiring prior data accumulation.

Event-based data processing systems can also be compared in terms of energy consumption. With Vivado software estimation, we determined that the total power usage for programmable logic utilised for each configuration ranges from 1.83 W (small model for $\beta = 128$) to 5.48 W (large model for $\beta = 256$). The estimated energy used by the PS part (ARM processor) is 2.74 W, regardless of the selected configuration and model. The achieved energy consumption values are higher than those obtained in [40] (1.81 W measured during runtime for FPGA fabric using the built-in power monitor controlled by the PMB). However, it is important to emphasise the differences in methodology (estimation vs measurement) as well as the fact that in [40] the representation generation in the processor part of the system is necessary (introducing additional energy requirement). For EvGNN [12], power consumption is reported only for the ASIC.

E. Comparison with embedded GPU

To evaluate the time and energy efficiency of our method compared to alternative embedded platforms, a reference implementation was created on the Jetson Orin NX eGPU platform. This system features an ARM Cortex-A78 processor and an NVIDIA Ampere GPU. Testing conditions similar to the FPGA configuration were reproduced by implementing a graph generator in C++, operating on a single CPU core. This generator reads events from the memory according to their timestamps, simulating the operation of a real event camera.

The resulting graph was then processed in parallel by the model on both CUDA and CPU platforms at two power levels: 10 W and 25 W. Figure 8 presents the average total power consumption and latency for all datasets. Due to the small size of the tested models, differences in processing times between EFGCN variants were minimal; therefore, a detailed analysis is provided only for the Base model.

Propagation times for models running on the CUDA platform ranged from 18.3 to 22.8 ms at 25 W and from 22.0 to 27.1 ms at 10 W for the CIFAR10-DVS, MNIST-DVS, and N-Cars datasets. Compared to the slowest hardware configuration (EFGCN-L with PL+PS mode), a speed-up of 2.6–3.2 and 3.0–3.9 times for FPGA was achieved, respectively. Additionally, the average graph generation time was 0.57–0.63 ms for the CPU on the Jetson platform, while FPGA implementation required only 75 μ s (15 clock cycles at a 200 MHz frequency). Considering this difference, the FPGA platform offers an overall speed-up of 7.6–8.4 \times with comparable energy consumption. Moreover, the average data transfer time from CPU to CUDA was 3.5 ms, introducing additional latency to the system.

Similar tests conducted exclusively on CPU-based models indicated even greater advantage of the FPGA implementation, achieving speed-ups of 18.9–127.8 times (25 W) and 20.4–139.9 times (10 W), with comparable graph generation times and without the need of data transfer to CUDA.

The presented results confirm the significant advantage of the proposed hardware implementation of graph convolutional networks over solutions utilising embedded GPU systems.

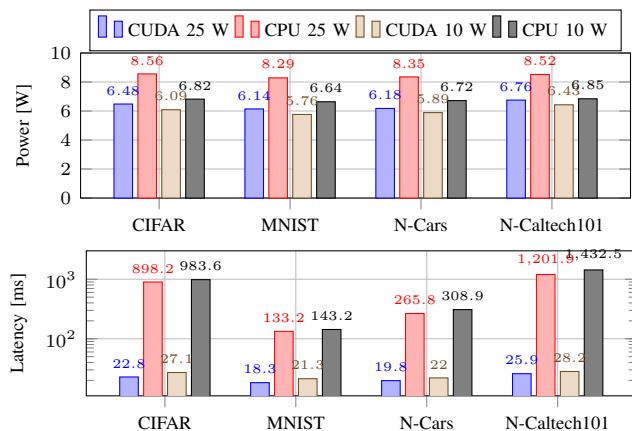


Fig. 8: Power consumption and latency for the Base model implemented on the Jetson Orin NX eGPU. As a reference, the power consumption for SoC FPGA Base model was estimated to be 4.79 W (for CIFAR, MNIST and N-Cars) and 7.15 W (for N-Caltech101).

VI. LIMITATIONS

In this section we define the current limitations of our system and outline the methods planned to address them with the further research on applying the accelerator to more complex computer vision tasks (e.g. object detection).

To increase data resolution and allow smaller temporal windows, a higher number of parallel multipliers is required. Consequently, the consumption of logic resources would increase. We plan to investigate techniques aimed at optimisation of multiplications (e.g. further utilisation of DSP resources with DSP packing). Additionally, we plan to explore the application of pruning techniques for the considered GCN model. Removing certain weights in the model would reduce both memory (sparse feature) and logic resource usage (fewer multiplications required for a given graph convolutional layer).

In the current implementation, we support only a fixed graph edge search radius of $R = 3$. We plan to evaluate the system for other values and conduct studies on their accuracy and efficiency. For more complex computer vision tasks, skip-connections are a widely used technique. We plan to integrate this mechanism by utilising external memory in a way that preserves the system's fixed latency. Furthermore, we are considering the implementation of a voxel-graph approach, where representing multiple events with a single node could significantly reduce the required memory and logic resources.

Finally, we plan to limit the use of the Processing System in order to further reduce both energy consumption and system latency. We aim to achieve this, by implementing the network's classification head with the AI Engines specific to the AMD Versal platform, instead of relying on the PS.

VII. SUMMARY

In this work, we present a hardware implementation of a graph convolutional neural network (GCNNs) for event data processing on a SoC FPGA platform. The developed system enables continuous event data processing, generating predictions for the last 50/100 ms (depending on the configuration)

while maintaining a fourfold increase in output frequency. Extensive evaluations across multiple models, configurations, and datasets demonstrate that the proposed approach outperforms existing methods in classification accuracy, computational efficiency, and hardware resource utilisation. Notably, our implementation operates without external memory, leading to reduced energy consumption. Moreover, we demonstrated the superior performance of the proposed hardware system compared to other platforms, namely the CPU and GPU.

Our solution surpasses state-of-the-art methods while offering high scalability. By leveraging the inherent temporal sparsity of event data and 3D MaxPool layers, we reduce FPGA logic utilisation through sequential computation of selected operations. Furthermore, the system establishes a direct trade-off between latency and resource utilisation – allowing for configuration adjustments that optimise one metric at the expense of the other, depending on the application's requirements.

As part of future work, we plan to introduce additional hardware optimisations, such as initial voxelisation of the graph, to significantly reduce both representation size and computational complexity. Additionally, we aim to integrate techniques that enhance the training process, including pruning and skip-connections. The ultimate goal is to develop a fully hardware-accelerated GCNN capable of real-time event-based object detection. This work addresses the application of our method for event-based vision, but it can also be used for other types of spatio-temporal point cloud data.

REFERENCES

- [1] F. K. Konstantinidis, S. G. Mouroutsos, and A. Gasteratos, "The role of machine vision in industry 4.0: an automotive manufacturing perspective," in *2021 IEEE International Conference on Imaging Systems and Techniques (IST)*, 2021, pp. 1–6.
- [2] L. Bodenhausen, A. R. Fugl, A. Jordt, M. Willatzen, K. A. Andersen, M. M. Olsen, R. Koch, H. G. Petersen, and N. Krüger, "An adaptable robot vision system performing manipulation actions with flexible objects," *IEEE transactions on automation science and engineering*, vol. 11, no. 3, pp. 749–765, 2014.
- [3] T.-H. Pham, A. Kheddar, A. Qammar, and A. A. Argyros, "Towards force sensing from vision: Observing hand-object interactions to infer manipulation forces," in *Proceedings of the IEEE conference on computer vision and pattern recognition*, 2015, pp. 2810–2819.
- [4] P. Lichtsteiner, C. Posch, and T. Delbruck, "A 128×128 120 db 15 μ s latency asynchronous temporal contrast vision sensor," *IEEE Journal of Solid-State Circuits*, vol. 43, no. 2, pp. 566–576, 2008.
- [5] S. Afshar, N. Ralph, Y. Xu, J. Tapson, A. v. Schaik, and G. Cohen, "Event-based feature extraction using adaptive selection thresholds," *Sensors*, vol. 20, no. 6, p. 1600, 2020.
- [6] R. Ghosh, A. Mishra, G. Orchard, and N. V. Thakor, "Real-time object recognition and orientation estimation using an event-based camera and cnn," in *2014 IEEE Biomedical Circuits and Systems Conference (BioCAS) Proceedings*, 2014, pp. 544–547.
- [7] E. Perot, P. De Tournemire, D. Nitti, J. Masci, and A. Sironi, "Learning to detect objects with a 1 megapixel event camera," *Advances in Neural Information Processing Systems*, vol. 33, pp. 16 639–16 652, 2020.
- [8] Y. Li, H. Zhou, B. Yang, Y. Zhang, Z. Cui, H. Bao, and G. Zhang, "Graph-based asynchronous event processing for rapid object recognition," in *Proceedings of the IEEE/CVF International Conference on Computer Vision*, 2021, pp. 934–943.
- [9] S. Schaefer, D. Gehrig, and D. Scaramuzza, "Aegnn: Asynchronous event-based graph neural networks," in *Proceedings of the IEEE/CVF conference on computer vision and pattern recognition*, 2022, pp. 12 371–12 381.
- [10] D. Gehrig and D. Scaramuzza, "Pushing the limits of asynchronous graph-based object detection with event cameras," *arXiv preprint arXiv:2211.12324*, 2022.

- [11] T. Kryjak, "Event-based vision on fpgas—a survey," *arXiv preprint arXiv:2407.08356*, 2024.
- [12] Y. Yang, A. Kneip, and C. Frenkel, "Evgnn: An event-driven graph neural network accelerator for edge vision," *arXiv preprint arXiv:1503.02531*, 2024.
- [13] Y. Sekikawa, K. Hara, and H. Saito, "Eventnet: Asynchronous recursive event processing," in *Proceedings of the IEEE/CVF conference on computer vision and pattern recognition*, 2019, pp. 3887–3896.
- [14] Q. Wang, Y. Zhang, J. Yuan, and Y. Lu, "Space-time event clouds for gesture recognition: From rgb cameras to event cameras," in *2019 IEEE Winter Conference on Applications of Computer Vision (WACV)*, 2019, pp. 1826–1835.
- [15] Y. Bi, A. Chadha, A. Abbas, E. Bourtsoulatz, and Y. Andreopoulos, "Graph-based object classification for neuromorphic vision sensing," in *Proceedings of the IEEE/CVF international conference on computer vision*, 2019, pp. 491–501.
- [16] A. Mitrokhin, Z. Hua, C. Fermüller, and Y. Aloimonos, "Learning visual motion segmentation using event surfaces," in *2020 IEEE/CVF Conference on Computer Vision and Pattern Recognition (CVPR)*, 2020, pp. 14402–14411.
- [17] K. Jeziorek, A. Pinna, and T. Kryjak, "Memory-efficient graph convolutional networks for object classification and detection with event cameras," in *2023 Signal Processing: Algorithms, Architectures, Arrangements, and Applications (SPA)*, 2023, pp. 160–165.
- [18] K. Jeziorek, P. Wzorek, K. Blachut, A. Pinna, and T. Kryjak, "Optimising graph representation for hardware implementation of graph convolutional networks for event-based vision," *arXiv preprint arXiv:2401.04988*, 2024.
- [19] W. Yan, W. Tong, and X. Zhi, "Fpgan: An fpga accelerator for graph attention networks with software and hardware co-optimization," *IEEE Access*, vol. 8, pp. 171 608–171 620, 2020.
- [20] N. Messikommer, D. Gehrig, A. Loquercio, and D. Scaramuzza, "Event-based asynchronous sparse convolutional networks," in *Computer Vision—ECCV 2020: 16th European Conference, Glasgow, UK, August 23–28, 2020, Proceedings, Part VIII 16*. Springer, 2020, pp. 415–431.
- [21] H. Rebecq, R. Ranftl, V. Koltun, and D. Scaramuzza, "High speed and high dynamic range video with an event camera," *IEEE transactions on pattern analysis and machine intelligence*, vol. 43, no. 6, pp. 1964–1980, 2019.
- [22] D. Gehrig, A. Loquercio, K. G. Derpanis, and D. Scaramuzza, "End-to-end learning of representations for asynchronous event-based data," in *Proceedings of the IEEE/CVF International Conference on Computer Vision*, 2019, pp. 5633–5643.
- [23] M. Cannici, M. Ciccone, A. Romanoni, and M. Matteucci, "Asynchronous convolutional networks for object detection in neuromorphic cameras," in *Proceedings of the IEEE/CVF Conference on Computer Vision and Pattern Recognition Workshops*, 2019, pp. 0–0.
- [24] A. Sabater, L. Montesano, and A. C. Murillo, "Event transformer: A sparse-aware solution for efficient event data processing," in *Proceedings of the IEEE/CVF Conference on Computer Vision and Pattern Recognition (CVPR) Workshops*, June 2022.
- [25] M. Gehrig and D. Scaramuzza, "Recurrent vision transformers for object detection with event cameras," in *Proceedings of the IEEE/CVF Conference on Computer Vision and Pattern Recognition (CVPR)*, 2023.
- [26] Y. Peng, Y. Zhang, Z. Xiong, X. Sun, and F. Wu, "Get: Group event transformer for event-based vision," in *Proceedings of the IEEE/CVF International Conference on Computer Vision*, 2023, pp. 6038–6048.
- [27] J. H. Lee, T. Delbruck, and M. Pfeiffer, "Training deep spiking neural networks using backpropagation," *Frontiers in neuroscience*, vol. 10, p. 508, 2016.
- [28] G. Orchard, C. Meyer, R. Etienne-Cummings, C. Posch, N. Thakor, and R. Benosman, "Hfirst: A temporal approach to object recognition," *IEEE transactions on pattern analysis and machine intelligence*, vol. 37, no. 10, pp. 2028–2040, 2015.
- [29] M. Gehrig, S. B. Shrestha, D. Mouritzen, and D. Scaramuzza, "Event-based angular velocity regression with spiking networks," in *2020 IEEE International Conference on Robotics and Automation (ICRA)*. IEEE, 2020, pp. 4195–4202.
- [30] M. Yao, H. Gao, G. Zhao, D. Wang, Y. Lin, Z. Yang, and G. Li, "Temporal-wise attention spiking neural networks for event streams classification," in *Proceedings of the IEEE/CVF International Conference on Computer Vision*, 2021, pp. 10 221–10 230.
- [31] L. Cordone, B. Miramond, and S. Ferrante, "Learning from event cameras with sparse spiking convolutional neural networks," in *2021 International Joint Conference on Neural Networks (IJCNN)*. IEEE, 2021, pp. 1–8.
- [32] S. Barchid, J. Mennesson, J. Eshraghian, C. Djéraba, and M. Benamoun, "Spiking neural networks for frame-based and event-based single object localization," *Neurocomputing*, vol. 559, p. 126805, 2023.
- [33] Y. Zhou, G. Gallego, X. Lu, S. Liu, and S. Shen, "Event-based motion segmentation with spatio-temporal graph cuts," *IEEE Transactions on Neural Networks and Learning Systems*, vol. 34, no. 8, pp. 4868–4880, 2021.
- [34] D. Gehrig and D. Scaramuzza, "Low-latency automotive vision with event cameras," *Nature*, vol. 629, no. 8014, pp. 1034–1040, 2024.
- [35] X. Lagorce, G. Orchard, F. Galluppi, B. E. Shi, and R. B. Benosman, "Hots: a hierarchy of event-based time-surfaces for pattern recognition," *IEEE transactions on pattern analysis and machine intelligence*, vol. 39, no. 7, pp. 1346–1359, 2016.
- [36] B. Ramesh, A. Ussa, L. Della Vedova, H. Yang, and G. Orchard, "Low-power dynamic object detection and classification with freely moving event cameras," *Frontiers in neuroscience*, vol. 14, p. 505328, 2020.
- [37] L. A. Camunas-Mesa, Y. L. Domínguez-Cordero, A. Linares-Barranco, T. Serrano-Gotarredona, and B. Linares-Barranco, "A configurable event-driven convolutional node with rate saturation mechanism for modular convnet systems implementation," *Frontiers in neuroscience*, vol. 12, p. 63, 2018.
- [38] J. Zhang, L. Feng, T. Wang, W. Shi, Y. Wang, and G. Zhang, "Fpga-based implementation of an event-driven spiking multi-kernel convolution architecture," *IEEE Transactions on Circuits and Systems II: Express Briefs*, vol. 69, no. 3, pp. 1682–1686, 2021.
- [39] A. Linares-Barranco, A. Rios-Navarro, S. Canas-Moreno, E. Piñero-Fuentes, R. Tapiador-Morales, and T. Delbruck, "Dynamic vision sensor integration on fpga-based cnn accelerators for high-speed visual classification," in *International Conference on Neuromorphic Systems 2021*, 2021, pp. 1–7.
- [40] Y. Gao, B. Zhang, Y. Ding, and H. K.-H. So, "A composable dynamic sparse dataflow architecture for efficient event-based vision processing on fpga," in *Proceedings of the 2024 ACM/SIGDA International Symposium on Field Programmable Gate Arrays*, 2024, pp. 246–257.
- [41] T. Dalgaty, T. Mesquida, D. Joubert, A. Sironi, P. Vivet, and C. Posch, "Hugnet: Hemi-spherical update graph neural network applied to low-latency event-based optical flow," in *Proceedings of the IEEE/CVF Conference on Computer Vision and Pattern Recognition (CVPR) Workshops*, June 2023, pp. 3953–3962.
- [42] M. Fey and J. E. Lenssen, "Fast graph representation learning with PyTorch Geometric," in *ICLR Workshop on Representation Learning on Graphs and Manifolds*, 2019.
- [43] C. R. Qi, L. Yi, H. Su, and L. J. Guibas, "Pointnet++: Deep hierarchical feature learning on point sets in a metric space," *Advances in neural information processing systems*, vol. 30, 2017.
- [44] B. Jacob, S. Kligys, B. Chen, M. Zhu, M. Tang, A. Howard, H. Adam, and D. Kalenichenko, "Quantization and training of neural networks for efficient integer-arithmetic-only inference," in *Proceedings of the IEEE conference on computer vision and pattern recognition*, 2018, pp. 2704–2713.
- [45] A. Sironi, M. Brambilla, N. Bourdis, X. Lagorce, and R. Benosman, "Hats: Histograms of averaged time surfaces for robust event-based object classification," in *Proceedings of the IEEE conference on computer vision and pattern recognition*, 2018, pp. 1731–1740.
- [46] G. Orchard, A. Jayawant, G. K. Cohen, and N. Thakor, "Converting static image datasets to spiking neuromorphic datasets using saccades," *Frontiers in neuroscience*, vol. 9, p. 159859, 2015.
- [47] H. Li, H. Liu, X. Ji, G. Li, and L. Shi, "Cifar10-dvs: An event-stream dataset for object classification," *Frontiers in Neuroscience*, vol. 11, 2017. [Online]. Available: <https://www.frontiersin.org/journals/neuroscience/articles/10.3389/fnins.2017.00309>
- [48] T. Serrano-Gotarredona and B. Linares-Barranco, "Poker-dvs and mnist-dvs. their history, how they were made, and other details," *Frontiers in Neuroscience*, vol. 9, 2015. [Online]. Available: <https://www.frontiersin.org/journals/neuroscience/articles/10.3389/fnins.2015.00481>
- [49] A. Paszke, S. Gross, S. Chintala, G. Chanan, E. Yang, Z. DeVito, Z. Lin, A. Desmaison, L. Antiga, and A. Lerer, "Automatic differentiation in pytorch," 2017.
- [50] D. P. Kingma, "Adam: A method for stochastic optimization," *arXiv preprint arXiv:1412.6980*, 2014.
- [51] M. Fey, J. E. Lenssen, F. Weichert, and H. Müller, "Splinecnn: Fast geometric deep learning with continuous b-spline kernels," in *Proceedings of the IEEE conference on computer vision and pattern recognition*, 2018, pp. 869–877.

Supplementary Material

VIII. MODEL DETAILS

TABLE VIII: Detailed architecture configurations of the three EFGCN model variants (Small, Base and Large).

Layer	Small	Base	Large
Conv1	1 + 3 → 16	1 + 3 → 16	1 + 3 → 16
3D MaxPool1	4 × 4 × 4	4 × 4 × 4	4 × 4 × 4
Conv2	16 + 3 → 32	16 + 3 → 32	16 + 3 → 32
Conv3	32 + 3 → 32	32 + 3 → 32	32 + 3 → 64
3D MaxPool2	2 × 2 × 2	2 × 2 × 2	2 × 2 × 2
Conv4	32 + 3 → 32	32 + 3 → 64	64 + 3 → 64
Conv5	32 + 3 → 32	64 + 3 → 64	64 + 3 → 128
PoolOut	4 × 4	4 × 4	4 × 4
Linear	16 × 32 → <i>cls</i>	16 × 64 → <i>cls</i>	16 × 128 → <i>cls</i>

As part of our research, we used three variants of the EFGCN model: Small, Base and Large. Each model consists of five convolutional layers, supplemented by two 3D MaxPool layers, and, after the final convolution, an additional PoolOut layer, which operates solely on the feature vectors of each node, selecting the maximum value from all nodes located within a defined spatial neighbourhood.

Table VIII presents detailed information about the models used. In the case of convolutional layers, the +3 notation refers to additional spatio-temporal event position features. For the 3D MaxPool layers, the given values define the voxel size in three dimensions. In the PoolOut layer, the operation is performed only in the spatial domain, resulting in just 2 values.

IX. FLOPS CALCULATION

In this section, we describe how we calculated the number of FLOPs performed by individual components of the convolution operation. Let:

- N denote the number of nodes in the graph,
- E denote the number of edges in the graph,
- K denote the average number of neighbours for an event in the graph,
- F_{in} and F_{out} denote the dimensions of the input and output data after the linear layer, respectively.

In this work, we used the PointNetConv layer, which consists of a single linear MLP layer called for each edge $e \in E$ in the graph. For a single edge, it requires multiplications and additions depending on the data dimensions:

$$FLOPS_{MLP} = 2 \times F_{in} \times F_{out} \quad (11)$$

Then, for each node in the graph, an aggregation is performed by computing the maximum value from all of its neighbours:

$$FLOPS_{Aggr} = F_{out} \times K \quad (12)$$

Finally, feature vector of node is updated, which requires one operation per data dimension:

TABLE IX: Ablation studies over different radius search for graph generation.

Model	Radius	N-Cars	N-Caltech101	CIFAR10-DVS	MNIST-DVS
EFGCN-S	3	0.907	0.623	0.571	0.964
EFGCN-B	3	0.920	0.631	0.588	0.978
EFGCN-L	3	0.923	0.639	0.613	0.983
EFGCN-S	5	0.929	0.665	0.623	0.979
EFGCN-B	5	0.941	0.673	0.631	0.985
EFGCN-L	5	0.947	0.688	0.654	0.991

$$FLOPS_{Updt} = F_{out} \quad (13)$$

Taking into account the entire graph and all operations, the total number of FLOPs can be expressed as:

$$\begin{aligned} FLOPS_{Tot} &= 2 \times F_{in} \times F_{out} \times E + F_{out} \times K \times E + F_{out} \times E \\ &= E \times (2 \times F_{in} \times F_{out} + F_{out} \times K + F_{out}) \\ &= E \times F_{out} \times (2 \times F_{in} + K + 1) \end{aligned}$$

The number of FLOPs per event was then determined by taking the total number of operations in the graph and averaging it over the number of events.

After the MaxPool operation, the values of the number of nodes N , the number of edges E , and the average number of neighbours K decreased accordingly, which led to a reduction in the number of FLOPs per event.

X. ADDITIONAL EXPERIMENTS

A. Radius distance

One of the key factors during graph generation is the neighbour search radius. Therefore, we conducted an ablation study to evaluate the effectiveness of our solution when using a larger radius. Following the example of other studies, where a radius of 5 was applied, we compared these results with our approach using a radius of 3. The outcomes of this comparison are summarised in Table IX.

The results clearly demonstrate that using a larger radius allows for improved performance. Comparing our findings with those reported in other works (Table VI in the main part of the paper), it can be observed that with an increased neighbour search radius, our Large model achieves higher accuracy than the AEGNN model on both datasets. Additionally, for the N-Cars dataset, our models achieved the highest accuracy among all compared approaches, while for the other datasets, the results approached the best reported values.

This confirms how significant the graph structure is for model performance and suggests that future research should also focus on increasing hardware representation capabilities.

TABLE X: Selection of parallel multiplication strategy for each layer of $\text{TIME_WINDOW} = 50$ ms models.

Model details			Small			Base			Large		
Layer	Graph <i>SIZE</i>	ΔT [μ s]	output <i>dim</i>	m	duration [μ s]	output <i>dim</i>	m	duration [μ s]	output <i>dim</i>	m	duration [μ s]
Conv 2	64	781.25	32	8	737.28	32	8	737.28	32	8	737.28
Conv 3	64	781.25	32	8	737.28	32	8	737.28	64	16	737.28
Conv 4	32	1562.5	32	1	1474.56	64	2	1474.56	64	2	1474.56
Conv 5	32	1562.5	32	1	1474.56	64	2	1474.56	128	4	1474.56

TABLE XI: Selection of parallel multiplication strategy for each layer of $\text{TIME_WINDOW} = 100$ ms models.

Layer	Graph <i>SIZE</i>	ΔT [μ s]	max output <i>dim</i>	m	duration [μ s]
Conv2	32	3125	32	1	1474.56
Conv3	32	3125	64	1	2949.12
Conv4	16	6250	64	1	737.28
Conv5	16	6250	128	1	1474.56

XI. SEQUENTIAL MULTIPLICATION STRATEGY

Tables X and XI present calculations conducted to determine the appropriate matrix multiplication parallelisation strategy for each synchronous layer across all supported models and configurations. The values in the table were determined with Equations (8)-(10) presented in the paper (Section IV.E).

For $\text{TIME_WINDOW} = 100$ ms, only the Large model was considered, as a single parallel multiplier ($m = 1$) is sufficient for all variants. In contrast, for $\text{TIME_WINDOW} = 50$ ms, we select the smallest possible value of m that ensures that the throughput requirements for each layer are still met.

XII. DETAILED RESOURCE UTILISATION

Tables XII and XIII provide a detailed resource utilisation analysis for individual modules in the EFGCN-B model with $\text{TIME_WINDOW} = 50$ ms and $\text{TIME_WINDOW} = 100$ ms configurations.

A. Memory utilisation

In the system, internal memory resources are utilised to store neural network weights (within the `u_sync_conv` modules) as well as feature maps between successive network layers (handled by the `u_feature_mem` modules – implemented using either UltraRAM or BRAM).

As the graph convolutional layers progress through the model, the feature vector dimensions increase, resulting in wider memory data widths. Simultaneously, subsequent 3D MaxPool layers reduce the size of the processed graph, thus decreasing the required memory depth.

B. Logic and DSP utilisation

The amount of logic resources used for a graph convolution depends on the number of parallel vector multiplication modules and the feature map dimensions. As a consequence, in the configuration with $\text{TIME_WINDOW} = 100$ ms – where each convolutional layer is implemented sequentially – each subsequent convolution consumes increasingly more resources due to the growing dimensionality of the feature vectors. In contrast, in the $\text{TIME_WINDOW} = 50$ ms configuration, the

TABLE XII: Resource utilisation for the EFGCN-B model on ZCU104 platform for $\text{TIME_WINDOW} = 50$ ms.

Module	LUT	FF	BRAM	URAM	DSP
GCN accelerator (sum)	138258	27176	185	12	184
GCN accelerator (usage)	60%	5.9%	59.3%	12.5%	10.7%
<code>u_gen_graph</code>	570	403	17	0	0
<code>u_async_conv1</code>	5411	1193	0	0	64
<code>u_maxpool1</code>	773	754	0	0	0
<code>u_feature_mem1</code>	517	14	49.5	0	0
<code>u_sync_conv2</code>	20849	4451	2.5	0	48
<code>u_feature_mem2</code>	1606	14	0	12	0
<code>u_sync_conv3</code>	40741	7413	4.5	0	48
<code>u_maxpool2</code>	931	1020	0	0	0
<code>u_feature_mem3</code>	1068	12	24	0	0
<code>u_sync_conv4</code>	8906	2893	4.5	0	12
<code>u_feature_mem4</code>	2363	12	45	0	0
<code>u_sync_conv5</code>	17347	4873	8	0	12
<code>u_maxpool3</code>	1563	1765	0	0	0
<code>u_feature_mem5</code>	1492	6	30	0	0
<code>u_out_serialise</code>	211	505	0	0	0

TABLE XIII: Resource utilisation for the EFGCN-B model on ZCU104 platform for $\text{TIME_WINDOW} = 100$ ms.

Module	LUT	FF	BRAM	DSP
GCN accelerator (sum)	51936	16210	159.5	88
GCN accelerator (usage)	22.5%	3.5%	51.1%	5%
<code>u_gen_graph</code>	515	398	5.5	0
<code>u_async_conv1</code>	5281	847	0	64
<code>u_maxpool1</code>	698	750	0	0
<code>u_feature_mem1</code>	698	12	13.5	0
<code>u_sync_conv2</code>	3812	1554	2.5	6
<code>u_feature_mem2</code>	603	12	24	0
<code>u_sync_conv3</code>	7651	2263	4	6
<code>u_maxpool2</code>	926	1014	0	0
<code>u_feature_mem3</code>	1322	10	24	0
<code>u_sync_conv4</code>	7115	2830	4	6
<code>u_feature_mem4</code>	1819	10	45	0
<code>u_sync_conv5</code>	10853	4264	7	6
<code>u_maxpool3</code>	1561	1764	0	0
<code>u_feature_mem5</code>	1940	6	30	0
<code>u_out_serialise</code>	131	440	0	0

highest logic resource utilisation is observed in the *Conv2* and *Conv3* layers. This is because they require as many as 16 (2×8) parallel vector multiplication units to handle relatively large feature map sizes of 32 and 64 elements, respectively.

DSP blocks are utilised exclusively for re-quantising 8-bit values following the multiplications. Their utilisation is determined solely by the adopted level of parallelism for the convolutions.